

Excitons and Trions in MoS₂ Quantum Dots: The Influence of the Dispersing Medium

Anna Thomas and Kochupurackal B. Jinesh*

Cite This: *ACS Omega* 2022, 7, 6531–6538

Read Online

ACCESS |



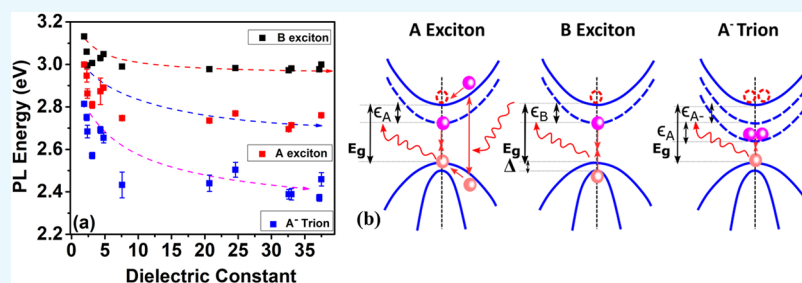
Metrics & More



Article Recommendations



Supporting Information



ABSTRACT: Single-layer MoS₂ has been reported to exhibit strong excitonic and trionic signatures in its photoluminescence (PL) spectra. Here, we report that the emission spectra of MoS₂ QDs strongly depend on the dielectric constant of the solvent and the relative difference in the electronegativity between the solvent and QDs. Due to the difference in electronegativity, electrons are either added to the QD or withdrawn from it. Consequently, depending upon the dielectric permittivity and the electronegativity of the surrounding medium, the signature peaks of excitons and trions exhibit a significant change in the PL spectra of MoS₂ QDs. Our findings are helpful to understand the effect of the surrounding environment on the optical properties of QDs and the importance of the selection of solvent since MoS₂ QDs are potential candidates for valleytronics applications.

1. INTRODUCTION

Two-dimensional materials such as graphene and transition-metal dichalcogenides (TMDCs) are attracting a great deal of attention due to their unique optical and electronic properties resulting from the confinement of charge carriers in two dimensions.¹ However, since graphene is semimetallic in nature with zero band gap, semiconducting TMDCs are of more importance for optoelectronic applications. Among such two-dimensional materials, molybdenum disulfide (MoS₂) has an indirect band gap of 1.2 eV in its bulk form. It turns into a direct band gap material with a band gap of 1.9 eV in the monolayer form.² The band gap is further tunable when MoS₂ is in the nanoparticle or quantum dot (QD) form due to the strong quantum confinement of charge carriers. In addition, MoS₂ QDs have interesting features such as large surface area, controllability in scaling in both lateral and vertical directions, good optical properties, biocompatibility, and strong hydrogen adsorption properties. Due to these peculiar features, MoS₂ QDs are useful in biological applications and hydrogen evolution reactions.^{3–5} Such quantum dots were often prepared by the liquid-phase exfoliation method,⁴ exfoliation based on Li-intercalation,⁶ electrochemical exfoliation, hydrothermal methods, and liquid-phase laser ablation.⁷

Several mechanisms that can modulate the optical and electronic properties of MoS₂ have been reported, which include covalent functionalization by phase engineering,⁸ modulation via photoinduced charge transfer,⁹ tunable photo-

luminescence properties via chemical doping,¹⁰ etc. If the synthesis method for the QDs is liquid-assisted exfoliation, the proper selection of the solvent can control the production yield and the respective properties.¹¹ It should be noted that unlike other QDs, MoS₂ QDs have no dangling bonds on their basal planes except at edges and defect sites.^{12,13} Therefore, most of the atoms of the QDs are exposed to the solvent in which they are suspended.^{12,14} As a result, these surrounding environments can play an important role in the optical properties of MoS₂ QDs. It is known that the many-body effects resulting from the Coulomb interactions influence the optical transitions in TMDCs,^{15,16} and such interactions are related to the dielectric constant of the surroundings.¹⁷ Therefore, the dielectric screening of the surrounding media will influence the behavior of quasiparticles (excitons and charge excitons, also called trions) in the optical transition. Choi et al.¹⁸ and Lin et al.¹⁷ have performed an elaborate study on the effect of dielectric screening effects of the surrounding media on the properties emanating from the quasiparticle confinements in

Received: September 30, 2021

Accepted: January 17, 2022

Published: February 16, 2022



monolayer MoS₂, charge transfer dynamics due to solvent effects in TMDC, etc. However, QDs are a versatile tool for band gap engineering, and such a detailed study on TMDC QDs has not been reported extensively in the literature.

In this work, we show the influence of the dielectric medium on the blue shift in the emission properties of MoS₂ QDs prepared by a simple liquid-phase exfoliation method. To study the effect of the surrounding media, MoS₂ QDs have been dispersed in various solvents with relative dielectric constants ranging from 1.85 to 37.5. We find that distinct peaks for charged and neutral excitons are visible in QDs prepared in lower dielectric media, which result from the charge transfer of the solvent to the QDs due to the relative difference in electronegativity. The observed blue shift in band gap calculated from absorption spectra in the low dielectric constant range is also attributed to the dielectric screening effect.

2. RESULTS AND DISCUSSION

The MoS₂ QDs were prepared in the following solvents: toluene, benzene, *N*-methyl-2-pyrrolidone (NMP), dimethylformamide (DMF), water, isopropyl alcohol (IPA), and acetone by the liquid-phase exfoliation method. To investigate the optical properties of MoS₂ QDs in different solvents, UV-vis spectra have been obtained.

Generally, the UV-vis spectrum of bulk MoS₂ exhibits two exciton absorption bands at around 672 nm (1.85 eV) and 615 nm (2.02 eV).¹⁹ These bands originate from the direct band gap transition at the K-point, and the energy splitting arises due to the valence band spin-orbital coupling.¹⁹ The peaks or the small shoulders observed near the UV region in Figure 1 are attributed to the strong quantum confinement effect in MoS₂ QDs.^{6,7} Figure S1 shows the image of Figure 1 in the 200–800 nm range, in which no absorption peaks are observed in the 600–800 nm region, and the spectra of our samples depict a substantial blue shift in the absorption peaks of the QDs. The respective band gaps of the QDs were calculated

using the Tauc plot²⁰ (see Figure S2) by assuming it as a direct band gap material and are tabulated in Table S1. The variation in the estimated band gap of QDs prepared in different solvents is attributed to the variations in the quantum dot size.

The representative transmission electron microscopy (TEM) images of QDs prepared in DMF and toluene are shown in Figure 2a,b. The particle size distribution shows that the average particle sizes are 3 and 7 nm in DMF and toluene, respectively. Figure 2c,d illustrates the active Raman modes of MoS₂. The in-plane (E_{2g}^1) mode corresponds to the two S atoms vibrating in the same direction and Mo atoms vibrating in the direction opposite to S atoms. However, in the out-of-plane (A_{1g}) mode, the two S atoms vibrate in the opposite way out of the plane and the Mo atom is stationary.²¹ Raman spectra of the samples are shown in Figure 2e, which were obtained in the ambient environment. For the bulk MoS₂ powder, it can be observed that the characteristic peaks E_{2g}^1 and A_{1g} at 374 and 400 cm⁻¹, respectively, correspond to the optical phonon modes. At the same time, for the exfoliated QDs, these distinct peaks blue-shifted to around 380 and 406 cm⁻¹, respectively. Usually, it has been found that the E_{2g}^1 vibration red shifts, while the A_{1g} vibration blue shifts with increasing sample thickness from monolayer to bulk.^{22,23} Our Raman results for the exfoliated sample reveal that both the characteristic Raman modes have become stiffened. This means that our samples are scaled down not only in the vertical direction but also in all three directions. As a result, both in-plane and out-of-plane vibrations are found to stiffen.²⁴ As the bulk MoS₂ was exfoliated to QDs, the E_{2g}^1 and A_{1g} peaks are observed to be blue-shifted due to the quantum confinement effects, which is consistent with the previous reports.^{24,25} The shift of A_{1g} mode is likely due to the decrease in the interlayer van der Waals interaction that causes weaker restoring forces in the vibration as MoS₂ becomes quantum dots.^{20,26} The shift of the E_{2g}^1 mode could be due to the reduced long-range Coulomb interaction between the effective charges caused by an increase in the dielectric screening on stacking-induced changes in the interlayer bonding.²⁶ The characteristic difference of Raman shifts between the E_{2g}^1 and A_{1g} peaks are found to be ~26 cm⁻¹ for QDs and the bulk MoS₂. The observation of a similar difference of 26 cm⁻¹ between the E_{2g}^1 and A_{1g} modes originates from the local symmetry of the MoS₂ because the local symmetry mostly remains unaltered even after the formation of QDs.²⁷

The signatures of excitonic transitions of MoS₂ are evident in its emission characteristics. Therefore, the PL spectra of MoS₂ QDs in different organic solvents were obtained, as shown in Figure 3 (see Figures S3–S8). We can observe the strong dependence of the excitation wavelength from these emission spectra, which can be attributed to the size heterogeneity commonly seen in transition-metal dichalcogenides.¹³ The PL spectra show two different types of emissions from the quantum dots. One type is from the MoS₂ QDs prepared in solutions with low dielectric constants, such as benzene and toluene, which depict multiple distinct peaks in the PL spectra. The other type of spectra is from MoS₂ QDs prepared in solutions with high dielectric constants, such as NMP and DMF, which had a single broad peak centered around 500 nm. The additional peaks present in the former one are assigned to the vibronic coupling to the high-frequency local vibrational modes, which may come from the edge bonds in the QDs.¹³

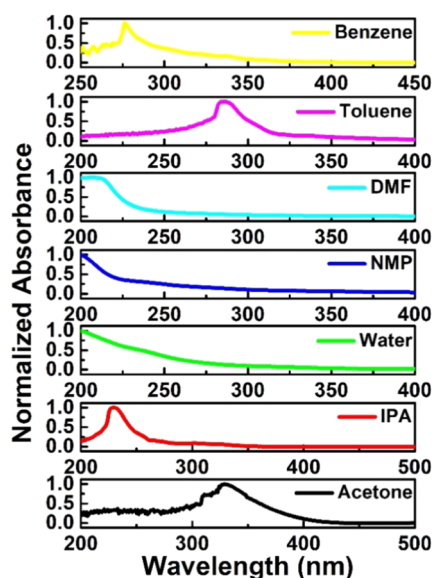


Figure 1. UV-vis absorption spectrum of MoS₂ QDs prepared in solvents such as toluene DMF, NMP, benzene, water, IPA, and acetone. Peaks or shoulders near the UV region represent the absorption peak's strong blue shift due to quantum confinement.

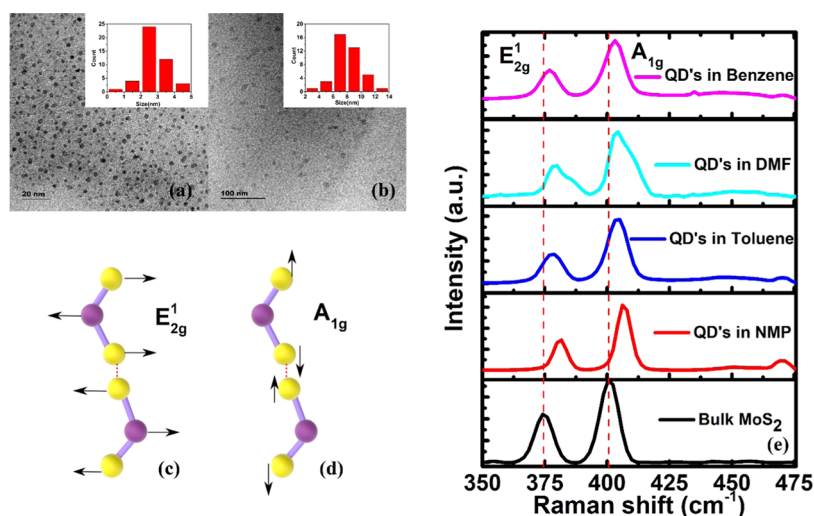


Figure 2. (a, b) Transmission electron microscopy (TEM) images of MoS₂ quantum dots prepared in DMF and toluene, respectively. Inset shows respective particle size distribution TEM analysis. (c, d) Illustration of Raman active modes of MoS₂ E_{2g}¹ and A_{1g}, respectively, gives the schematic representations of in-plane and out-of-plane vibrations of Mo and S atoms. (e) Raman spectra MoS₂ bulk and QDs, showing the in-plane (E_{2g}¹) and out-of-plane (A_{1g}) vibrational modes of the S atoms.

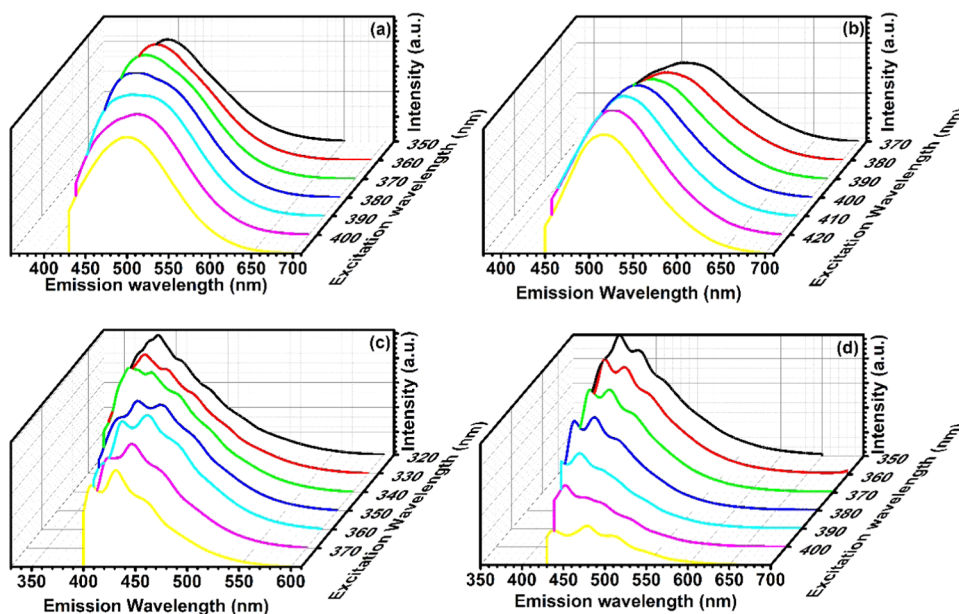


Figure 3. Photoluminescent spectrum of liquid-phase exfoliated QDs in (a) DMF, (b) NMP, (c) benzene, and (d) toluene.

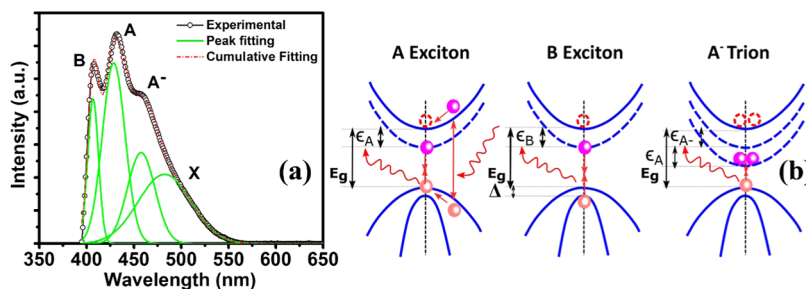


Figure 4. (a) Typical PL spectrum of MoS₂ QDs prepared in toluene. The black circles represent the experimental data, and the green lines represent the fitting of peaks. The red dotted line is the cumulative fitting. The peaks are fitted with a Gaussian peak fitting with an R^2 value of 0.999. (b) Diagram of the generation and recombination of the exciton and the trion. Here, E_g is the band gap, Δ is the valence band splitting, and ϵ_A , ϵ_B , and ϵ_{A^-} denote the binding energy of A exciton, B exciton, and A⁻ trions, respectively.

To interpret the multiple PL peaks in MoS₂ QDs, the PL spectrum has been deconvoluted by fitting with four Gaussian

peaks. The multiple peaks appearing in the PL spectra correspond to the optical transitions of A exciton,

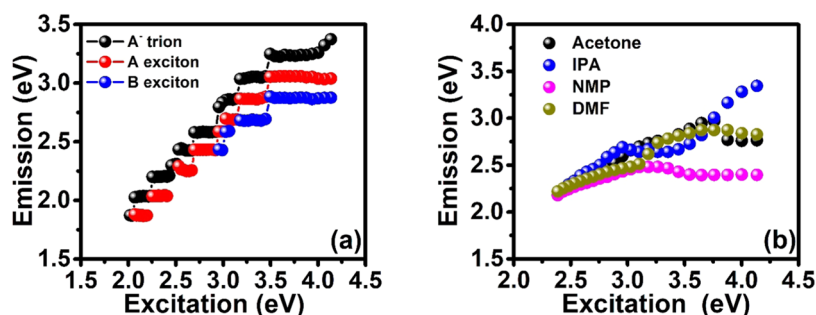


Figure 5. (a) Emission energy is plotted as a function of excitation energy for QDs prepared in toluene. Black, red, and blue dots correspond to A⁻ trions, A exciton, and B exciton. (b) Emission energy is plotted as a function of excitation energy for QDs prepared in acetone, ethanol, IPA, water, NMP, and DMF.

and A⁻ trions (“charged” excitons, i.e., the bound state of two electrons and a hole or two holes and one electron) and the defect-bound exciton (X) respectively.¹⁷ The detailed extraction of the peaks is shown in Figure 4, in which a typical PL spectrum of QDs dispersed in toluene is studied. The spectrum was fitted with three peaks that originated from the radiative recombinations of B exciton, A exciton, and A⁻ trions, respectively. The presence of strong radiative recombinations of trions in MoS₂ is consistent with our result.^{17,28,29}

Figure 4b illustrates the radiative recombination of A exciton, B exciton, and A⁻ trions at the K-point of the Brillouin zone. While the A exciton is formed by the Coulomb interaction between a hole from the top of the valence band (VB) and an electron from the bottom of the conduction band (CB), the B exciton is formed by the Coulomb interaction of a hole from the lower level of the split VB and an electron from the bottom of the CB. Similarly, A⁻ trions are formed by the Coulomb interaction of an A exciton and an electron. And the X exciton peak is assigned to the radiative recombination of bound excitons from the trap states.³⁰

The PL peak energy of direct band gap semiconductors, i.e., the optical band gap, is equal to the difference between the electronic band gap calculated from the electronic dispersion relation and the binding energy of the quasiparticles originating from the Coulomb interaction between electrons and holes. Lin et al.¹⁷ have reported the detailed expression for PL peak energies of A exciton, B exciton, and A⁻ trions for monolayer MoS₂. As seen in the previous reports, the emission peak energy corresponding to the trion, A exciton, and B exciton for a monolayer MoS₂ was found to be 1.77 eV (633 nm), 1.81 eV (683 nm), and 1.96 eV (700 nm), respectively.³¹ But, in this present work, QD emissions were centered around the 400–500 nm region, which is due to the size reduction and quantum confinement. As a result, trion and excitonic emission peaks blue shift with a decrease in the layer number or size of the QDs.³² Therefore, in the case of QDs, additional confinement energy terms also have to be added to the PL peak energies and are given as follows

$$PL_A = E_g - \epsilon_A + E_{\text{confinement}} \quad (1)$$

$$PL_B = E_g + \Delta - \epsilon_B + E_{\text{confinement}} \quad (2)$$

$$PL_{A^-} = E_g - \epsilon_A - \epsilon_{A^-} + E_{\text{confinement}} \quad (3)$$

From the above equations, one can understand the direct correlation between quasiparticle binding energy and PL peak energies. The addition of confinement energy causes the blue shift of emission spectra compared to the few-layer or bulk

MoS₂, which is clearly visible in Figure 3. While plotting the emission peak energy as a function of excitation energy (see Figures 5a,b and S9), QDs prepared in toluene and benzene follow a distinct trend as compared to QDs prepared in other solvents. The PL peaks of B exciton, A exciton, and A⁻ trions follow a steplike behavior with a step size of ~200 meV. There could be two possible reasons for this: first, the density of states (DOS) of a monolayer or bilayer MoS₂ follows that of a two-dimensional electron gas because of the confinement in the Z direction.³³ Since QDs are zero-dimensional relative to the bulk, the DOS depends upon how QDs are arranged or, in other words, whether or not they are aggregated. Therefore, as reported earlier, for a series of QDs, the electronic charges in the QDs cause repulsion to another charge and it leads to a steplike DOS in aggregates.³⁴ It implies that in the case of QDs arranged in series, it acts similar to a 2D electron gas system. Therefore, the energy will be proportional to the quantum number *n*.

It is rather surprising that the three excitonic peaks appear in QDs prepared in toluene-like solvents but not in QDs prepared in DMF-like solvents. At this point, it is crucial to consider the effect of the surrounding environment of QDs or the proper selection of solvent for the preparation of the QDs for tuning the optical properties. Taking the case of graphene, Srivastava et al.¹¹ suggest that the dielectric environment acted as a key factor in enhancing the production yield in the exfoliation process. Similarly, the exfoliation of MoS₂ will be different in both solutions. According to Hernandez et al.,³⁵ for the liquid-phase exfoliation to occur, the net energy cost or, in other words, the enthalpy of mixing should be very small. In our case, the enthalpy of mixing $\Delta H \propto (S_{\text{MoS}_2} - S_{\text{solvent}})^2$, where S_{MoS_2} and S_{solvent} are the surface energies of MoS₂ and solvent. S_{MoS_2} is defined as the energy per unit area required to overcome the van der Waals force when separating two MoS₂ sheets apart.¹¹ It is clear from the equation that the minimal energy will be spent for exfoliation if the surface energy of the solvents matches that of MoS₂. The surface energy of MoS₂ was 46.5 mJ/m²,³⁶ and those for DMF and toluene were 68 and 59 mJ/m².¹¹ Since both solutions have their surface energy almost in the range of MoS₂, the net energy cost will be almost the same.

If the surface energy solely governs the visible presence of exciton nodes in the toluene, the same should be observed in DMF as well but are absent in DMF. This indicates that there are other parameters also involved in the appearance of the excitonic peaks in the emission spectra of the QDs.

To elucidate the influence of the solvent in the PL spectra of the MoS₂ QDs, some of the parameters such as electro-

negativity and dielectric constant were examined. Electronegativity, being a measure of the tendency of a medium to attract electrons, will determine which of the two interacting molecular systems will become electron donors or acceptors.³⁷ According to the difference in electronegativity, electron transfer will occur from the solvent to the QDs or vice versa. The electronegativity is expressed as $\chi = \frac{1}{2}(\text{IP} + \text{EA})$, where IP is the ionization potential and EA is the electron affinity.³⁷ Using the above expression, the electronegativity of DMF has been calculated to be 4.57 eV, and for toluene, it has been calculated to be 3.86 eV.¹⁸ The electronegativity values of MoS₂ have been obtained from the literature ($\chi_{\text{MoS}_2} = 5.06\text{--}5.2$ eV).¹⁸

To study the effect of the solvent's electronegativity on PL spectra, the MoS₂ QD sample prepared in toluene was vacuum dried and dispersed again in DMF. To confirm that drying does not affect the properties, the absorption spectrum of dried MoS₂ QDs was obtained, as shown in Figure S10. The absorption spectrum does not exhibit much change, as compared to Figure 1, indicating that drying does not change the QD properties. The corresponding PL spectra of the redispersed QD at different excitation wavelengths are shown in Figure S11. One such PL spectrum is shown in Figure 6. It

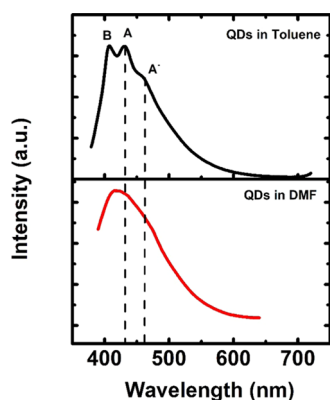


Figure 6. Typical photoluminescent spectrum of MoS₂ QDs prepared in toluene at 370 nm excitation is shown in black lines. The peaks correspond to A⁻ trions, A exciton, and B exciton. The red line in the graph represents the PL spectrum of MoS₂ QDs prepared in toluene, which was vacuum dried and redispersed in a DMF solution. Interestingly, the excitonic and trionic peaks have quenched in the latter.

can be observed that the intensity ratio of trion to exciton varies from QDs in toluene to the QDs redispersed in DMF. The intensity ratio of A⁻ trion to A exciton reduced from 93.9 to 71.2%. To confirm that the drying process does not have any influence, the PL spectrum of QDs prepared in toluene that had been dried and redispersed in toluene obtained at 370 nm excitation is shown in Figure S12. Significant peaks corresponding to excitons and trions indicate that there is no formation of aggregates. If two systems with different electronegativity interact with each other, the medium with higher electronegativity withdraws electrons from the other until the associated chemical potential reaches equilibrium.³⁷ In our case, if we are considering the electronegativity values of toluene, MoS₂, and DMF, the MoS₂ QDs will attract more electrons from toluene than from DMF because of the higher electronegativity values of MoS₂ QDs. This electron transfer will result in changes in the intensity of the PL spectrum. As a result, there will be an increase in the electron density in MoS₂ QDs, which leads to PL quenching, which causes destabilized exciton recombination by an increased formation of charged excitons, i.e., A⁻ trions. A similar mechanism has been observed, such as tunable PL properties of single-layer MoS₂, using a molecular chemical doping technique where the PL intensity of single-layer MoS₂ was drastically enhanced by the adsorption of p-type dopants¹⁰ and electron doping via surface functionalization, where the adsorbed molecule ultimately modulates the emission characteristics.³⁸

It is important to note that the PL peak energy described in equations earlier, i.e., the optical band gap, is equal to the difference between the electronic band gap and the binding energy of the quasiparticles originating from the Coulomb interaction between electrons and holes. The binding energy of the quasiparticle (trions and excitons) corresponds to the Coulomb interaction between negatively charged electrons and holes. This Coulomb potential distribution is strongly screened by the dielectric environments. The dielectric-screened Coulomb potential for the electron and hole separated by a distance L can be expressed as¹⁷ $V_{2D}(L) = \frac{e^2}{\epsilon_0 \kappa_{\text{eff}} L_0} f\left(\frac{L}{L_0}\right)$, where ϵ_0 is the vacuum permittivity, e the electronic charge, κ_{eff} is the effective dielectric constant, L_0 is the screening length, and $f(L/L_0)$ is a dimensionless function. Also, the exciton binding energy has a scaling relationship with the surrounding effective dielectric constant, i.e., $\epsilon_X = \epsilon_{X0} (\kappa_{\text{eff}})^{-\alpha_X}$, where ϵ_{X0} is the binding energy in vacuum and α_X is the empirical scaling factor, X represents A exciton, B exciton, and A⁻ trions.¹⁷

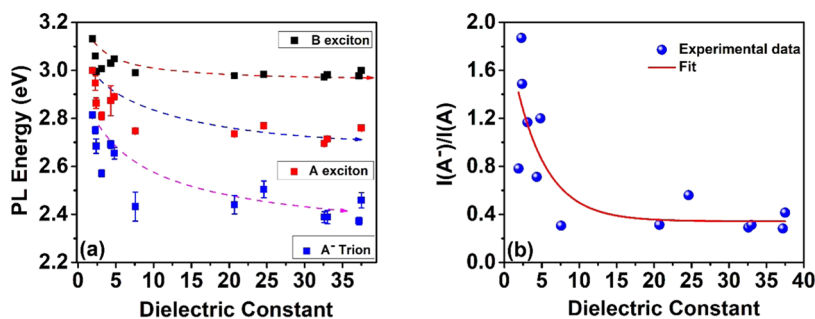


Figure 7. (a) Emission energy plotted for MoS₂ QDs in various solvents as a function of the dielectric constant. Here, blue, red, and black squares correspond to the PL emission energy of A⁻ trions, A exciton, and B exciton, respectively. (b) Dependence of the A⁻/A intensity ratio on the dielectric constant of the surrounding media. Here, blue dots represent the experimental data, and the red line represents the exponential fit. The fitting has been done with double exponential decay function with an adjusted R^2 value of 0.85.

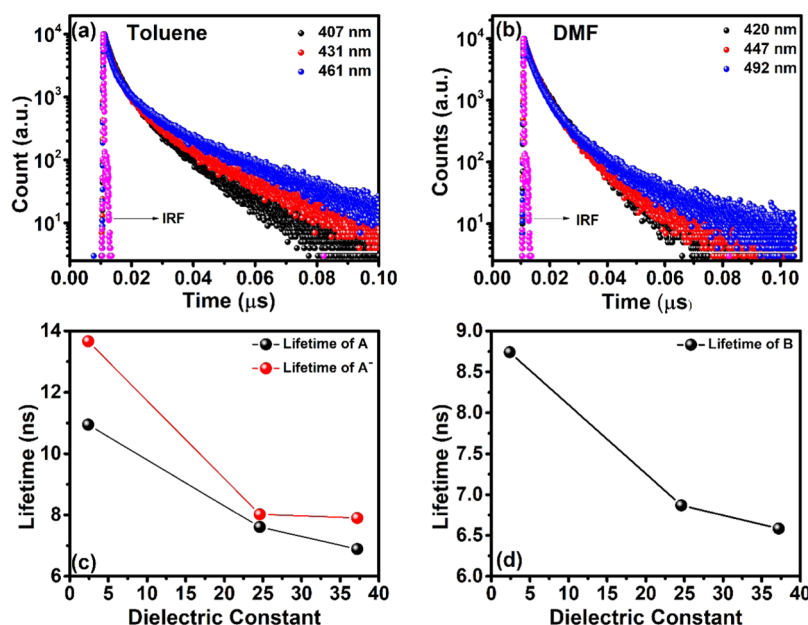


Figure 8. Lifetime decay of MoS₂ QDs prepared in toluene and redispersed in (a) toluene and (b) DMF. Here black, red, and blue dots correspond to the lifetime decay of to A⁻ trions, A exciton, and B exciton, respectively, at an excitation of 375 nm. (c, d) Average lifetime of excitons in MoS₂ QDs in different dielectric media. (c) Average lifetime of A exciton and A⁻ trion, and (d) B exciton.

From these expressions, we can find the relation between the dielectric constant of the surroundings and the binding energy of the quasiparticles. At the same time, PL peak energies of the quasiparticles are also directly related to the binding energy.

To study the effect of dielectric constants of the surrounding media on the quasiparticle emission energy, QDs prepared in toluene have been dried and dispersed in solvents of different dielectric constants, and the corresponding set of emissions is shown in Figure S13. The respective PL energy corresponding to A⁻ trions, A exciton, and B exciton at an excitation wavelength of 370 nm with a varying dielectric constant is shown in Figure 7. It can be observed that from ϵ_r 1.89 (hexane) to 7.58 (THF), the PL peak energies shift faster, and from ϵ_r 20.7 (acetone) onward, the peak energies become almost constant, i.e., there is no significant shift after that. Also, it should be noted that the emission energy of A⁻ trions shifts faster than that of A exciton. That means the trion binding energy increases with an increase in the dielectric constant since $PL_{A^-} - PL_A = \epsilon_{A^-}$. Similar to the PL peak energy, the intensity ratio of trions to excitons can be tuned by the surrounding dielectric. From the mass action model reported previously,¹⁷ the intensity ratio can be derived as $\frac{I(A^-)}{I(A)} = K(\kappa_{\text{eff}})^\delta \exp\left(\frac{\epsilon_{A^-}}{\kappa_{\text{eff}} T}\right)$, where K and δ are the fitting parameters and $\frac{\Gamma_{A^-}}{\Gamma_A} \propto (K_{\text{eff}})^\delta$, where Γ_{A^-} and Γ_A are the radiative recombination rates. As seen in Figure 7b, it can be observed that the A⁻/A intensity ratio decreases with an increase in the dielectric permittivity of the surrounding medium. The A⁻/A intensity ratio drops from 1.89 to 0.4 as the dielectric constant varies from 1.89 to 37.5. Theoretically, it means that the radiative recombination rate of A exciton changes faster with environmental dielectric than that of the radiative recombination rate of A⁻ trion.

To confirm whether the radiative recombination rate of A exciton changes faster with environmental dielectric than that of A⁻ trion, we have done the lifetime decay measurements of

MoS₂ QDs in the different dielectric environments. The measurement is done in such a way that the lifetime decay has been measured at three emission wavelengths, which correspond to the A exciton, B exciton, and A⁻ trion for each sample. Even though there will be overlapping emission peaks corresponding to trions and excitons, the maximum probable emission arises from the respective quasiparticle while choosing the particular wavelength. However, the wavelength chosen accounts for the trion binding energy of the order 100 meV ($PL_{A^-} - PL_A = \epsilon_{A^-}$). In the case of monolayer MoS₂, the trion binding energy is reported to be 20 meV.²⁹ However, when QDs are formed, due to the addition of quantum confinement, it will likely increase the trion binding energy.^{39–41}

Figure 8 shows the lifetime measurements of the QDs redispersed in (Figure 8a) toluene, DMF (Figure 8b), and ethanol (Figure S14). The average lifetime has been extracted using IRF-included exponential fitting.⁴² Details regarding the fitting and the three components are given in Table S2. The extracted lifetime with respect to the dielectric constant is plotted in Figure 8c,d. As evident from the figure, the extracted lifetime corresponding to the A⁻ trion tends to saturate after the dielectric constant of 24.6. At the same time, the extracted lifetime corresponding to A exciton tends to reduce with the increase in the dielectric constant of the solvents. It implies that the average lifetime of A exciton changes faster than that of A⁻ trion. Since the lifetime and radiative recombination are directly related, one can say that the radiative recombination rate of A exciton will be faster than that of the trion, which validates our arguments regarding the dielectric dependence of the intensity ratio of trions to excitons.

3. CONCLUSIONS

The dielectric permittivity of the medium that surrounds the MoS₂ QDs has a significant influence on the emission properties of the QDs. We find that the surrounding medium donates electrons to the QDs, which in effect causes

destabilized exciton recombination by an increased formation of A^- trions. Also, we find that the PL peak energies of A^- trions shift faster than those of A exciton with respect to the increase in the dielectric constant. And the radiative recombination rate of A exciton changes more quickly with dielectric permittivity than that of the A^- trions. Moreover, we can control the generation of A^- trion and A exciton by properly tuning and selecting the surrounding environment. This will be a valuable information for tuning the emission properties of TMDC QDs for various optoelectronics and valleytronics applications.

4. EXPERIMENTAL METHODS

We employed the liquid-phase exfoliation method for the preparation of MoS_2 QDs. MoS_2 powder (Sigma-Aldrich) was mixed with the intended solvent in a ratio of 1 g/100 mL and probe-sonicated for 3 h. The solvents used were DMF, NMP, IPA, acetone, water, toluene, and benzene. The sonicated dispersion was again stirred using a magnetic stirrer at a temperature below the boiling point of the respective solvent for 6 h. Afterward, this dispersion was centrifuged to filter out the sediments. The resultant supernatants containing QD suspensions were used for further characterizations.

To study the dielectric dependence, MoS_2 QDs prepared in toluene was vacuum dried at 240 mbar pressure at 60 °C and redispersed in solvents such as hexane ($k = 1.89$), benzene ($k = 2.28$), toluene ($k = 2.38$), ethyl acetate ($k = 3.099$), diethyl ether ($k = 4.33$), chloroform ($k = 4.81$), THF ($k = 7.58$), acetone ($k = 20.7$), ethanol ($k = 24.6$), methanol ($k = 32.6$), NMP ($k = 33$), DMF ($k = 37.2$), and acetonitrile ($k = 37.5$).

The UV–vis absorption spectrum of the MoS_2 quantum dots was measured using a Cary 100 Bio UV spectrometer. Raman spectra of the molecular vibrational levels were studied using a HORIBA Scientific-Jobin Yvon Technology Raman spectrometer with 532 nm laser with a laser power of 50 mW, and the photoluminescence measurements were taken using a HORIBA Scientific FluoroMax-4 spectrometer. The transmission electron micrographs were taken using a JEOL JEM 2100 high-resolution electron microscope, with a maximum acceleration voltage of 200 kV. The lifetime measurement was carried out using an IBH FluoroCube time-correlated picosecond single-photon counting (TCSPC) system. The samples were excited using a diode laser of 375 nm (<100 ps pulse duration) with a repetition rate of 250 kHz.

■ ASSOCIATED CONTENT

SI Supporting Information

The Supporting Information is available free of charge at <https://pubs.acs.org/doi/10.1021/acsomega.1c05432>.

UV–vis absorption spectroscopy of MoS_2 QDs in the range of 200–800 nm showing the blue shift of absorption peaks; band gap estimation using Tauc plot analysis of QDs; calculated band gap of MoS_2 QDs prepared in different solvents; the photoluminescent spectrum of liquid-phase exfoliated QDs in DMF, NMP, benzene, toluene, IPA, and acetone; emission energy plotted as a function of excitation energy for QDs prepared in toluene; the UV absorption spectrum of dried MoS_2 QDs; the photoluminescence spectrum of MoS_2 QDs prepared in toluene redispersed in DMF; emission spectra of QDs prepared in toluene and redispersed in toluene; the photoluminescence spectrum

of MoS_2 QDs prepared in toluene redispersed in different solvents having varying dielectric constants; lifetime decay measurements of MoS_2 QDs dispersed in ethanol; and details regarding the calculation of average lifetime and fluorescence decay components of MoS_2 QD redispersed in three different solvents (PDF)

■ AUTHOR INFORMATION

Corresponding Author

Kochupurackal B. Jinesh – Department of Physics, Indian Institute of Space-Science and Technology (IIST), Thiruvananthapuram 695547 Kerala, India; orcid.org/0000-0003-4396-0880; Email: kbjinesh@iist.ac.in

Author

Anna Thomas – Department of Physics, Indian Institute of Space-Science and Technology (IIST), Thiruvananthapuram 695547 Kerala, India; orcid.org/0000-0002-8153-5722

Complete contact information is available at:

<https://pubs.acs.org/10.1021/acsomega.1c05432>

Notes

The authors declare no competing financial interest.

■ REFERENCES

- (1) Wang, Q. H.; et al. Electronics and Optoelectronics of Two-Dimensional Transition Metal Dichalcogenides. *Nat. Nanotechnol.* **2012**, *7*, 699–712.
- (2) Ellis, J. K.; Lucero, M. J.; Scuseria, G. E. The Indirect to Direct Band Gap Transition in Multilayered MoS_2 as Predicted by Screened Hybrid Density Functional Theory. *Appl. Phys. Lett.* **2011**, *99*, No. 261908.
- (3) Guo, Y.; Li, J. MoS_2 Quantum Dots: Synthesis, Properties and Biological Applications. *Mater. Sci. Eng. C* **2020**, *109*, No. 110511.
- (4) Arul, N. S.; Nithya, V. D. Molybdenum Disulfide Quantum Dots: Synthesis and Applications. *RSC Adv.* **2016**, *6*, 65670–65682.
- (5) Benson, J.; Li, M.; Wang, S.; Wang, P.; Papakonstantinou, P. Electrocatalytic Hydrogen Evolution Reaction on Edges of a Few Layer Molybdenum Disulfide Nanodots. *ACS Appl. Mater. Interfaces* **2015**, *7*, 14113–14122.
- (6) Qiao, W.; Yan, S.; Song, X.; Zhang, X.; He, X.; Zhong, W.; Du, Y. Luminescent Monolayer MoS_2 Quantum Dots Produced by Multi-Exfoliation Based on Lithium Intercalation. *Appl. Surf. Sci.* **2015**, *359*, 130–136.
- (7) Li, B.; Jiang, L.; Li, X.; Ran, P.; Zuo, P.; Wang, A.; Qu, L.; Zhao, Y.; Cheng, Z.; Lu, Y. Preparation of Monolayer MoS_2 Quantum Dots Using Temporally Shaped Femtosecond Laser Ablation of Bulk MoS_2 Targets in Water. *Sci. Rep.* **2017**, *7*, No. 11182.
- (8) Voiry, D.; Goswami, A.; Kappera, R.; de Carvalho Castro e Silva, C.; Kaplan, D.; Fujita, T.; Chen, M.; Asefa, T.; Chhowalla, M. Covalent Functionalization of Monolayered Transition Metal Dichalcogenides by Phase Engineering. *Nat. Chem.* **2015**, *7*, 45–49.
- (9) Choi, J.; Zhang, H.; Choi, J. H. Modulating Optoelectronic Properties of Two-Dimensional Transition Metal Dichalcogenide Semiconductors by Photoinduced Charge Transfer. *ACS Nano* **2016**, *10*, 1671–1680.
- (10) Mouri, S.; Miyauchi, Y.; Matsuda, K. Tunable Photoluminescence of Monolayer MoS_2 via Chemical Doping. *Nano Lett.* **2013**, *13*, 5944–5948.
- (11) Srivastava, P. K.; Yadav, P.; Ghosh, S. Dielectric Environment as a Factor to Enhance the Production Yield of Solvent Exfoliated Graphene. *RSC Adv.* **2015**, *5*, 64395–64403.
- (12) Yu, Z.; et al. Towards Intrinsic Charge Transport in Monolayer Molybdenum Disulfide by Defect and Interface Engineering. *Nat. Commun.* **2014**, *5*, No. 5290.

- (13) Jin, H.; Baek, B.; Kim, D.; Wu, F.; Batteas, J. D.; Cheon, J.; Son, D. H. Effects of Direct Solvent-Quantum Dot Interaction on the Optical Properties of Colloidal Monolayer WS₂ Quantum Dots. *Nano Lett.* **2017**, *17*, 7471–7477.
- (14) Sim, D. M.; Kim, M.; Yim, S.; Choi, M.-J.; Choi, J.; Yoo, S.; Jung, Y. S. Controlled Doping of Vacancy-Containing Few-Layer MoS₂ via Highly Stable Thiol-Based Molecular Chemisorption. *ACS Nano* **2015**, *9*, 12115–12123.
- (15) Berkelbach, T. C.; Hybertsen, M. S.; Reichman, D. R. Theory of Neutral and Charged Excitons in Monolayer Transition Metal Dichalcogenides. *Phys. Rev. B* **2013**, *88*, No. 045318.
- (16) Komsa, H.-P.; Krasheninnikov, A. V. Effects of Confinement and Environment on the Electronic Structure and Exciton Binding Energy of MoS₂ from First Principles. *Phys. Rev. B* **2012**, *86*, No. 241201.
- (17) Lin, Y.; Ling, X.; Yu, L.; Huang, S.; Hsu, A. L.; Lee, Y.-H.; Kong, J.; Dresselhaus, M. S.; Palacios, T. Dielectric Screening of Excitons and Trions in Single-Layer MoS₂. *Nano Lett.* **2014**, *14*, 5569–5576.
- (18) Choi, J.; Zhang, H.; Du, H.; Choi, J. H. Understanding Solvent Effects on the Properties of Two-Dimensional Transition Metal Dichalcogenides. *ACS Appl. Mater. Interfaces* **2016**, *8*, 8864–8869.
- (19) Siegel, G.; Venkata Subbaiah, Y. P.; Prestgard, M. C.; Tiwari, A. Growth of Centimeter-Scale Atomically Thin MoS₂ Films by Pulsed Laser Deposition. *APL Mater.* **2015**, *3*, No. 056103.
- (20) Hazarika, S. J.; Mohanta, D. Inorganic Fullerene-Type WS₂ Nanoparticles: Processing, Characterization and Its Photocatalytic Performance on Malachite Green. *Appl. Phys. A* **2017**, *123*, No. 381.
- (21) Molina-Sánchez, A.; Wirtz, L. Phonons in Single-Layer and Few-Layer MoS₂ and WS₂. *Phys. Rev. B* **2011**, *84*, No. 155413.
- (22) Li, H.; Zhang, Q.; Yap, C. C. R.; Tay, B. K.; Edwin, T. H. T.; Olivier, A.; Baillargeat, D. From Bulk to Monolayer MoS₂: Evolution of Raman Scattering. *Adv. Funct. Mater.* **2012**, *22*, 1385–1390.
- (23) Lee, C.; Yan, H.; Brus, L. E.; Heinz, T. F.; Hone, J.; Ryu, S. Anomalous Lattice Vibrations of Single- and Few-Layer MoS₂. *ACS Nano* **2010**, *4*, 2695–2700.
- (24) Mukherjee, S.; Maiti, R.; Midya, A.; Das, S.; Ray, S. K. Tunable Direct Bandgap Optical Transitions in MoS₂ Nanocrystals for Photonic Devices. *ACS Photonics* **2015**, *2*, 760–768.
- (25) Nguyen, T. P.; Sohn, W.; Oh, J. H.; Jang, H. W.; Kim, S. Y. Size-Dependent Properties of Two-Dimensional MoS₂ and WS₂. *J. Phys. Chem. C* **2016**, *120*, 10078–10085.
- (26) Xu, Y.; Yan, L.; Li, X.; Xu, H. Fabrication of Transition Metal Dichalcogenides Quantum Dots Based on Femtosecond Laser Ablation. *Sci. Rep.* **2019**, *9*, No. 2931.
- (27) Reshmi, S.; Akshaya, M. V.; Satpati, B.; Roy, A.; Kumar Basu, P.; Bhattacharjee, K. Tailored MoS₂ Nanorods: A Simple Microwave Assisted Synthesis. *Mater. Res. Express* **2017**, *4*, No. 115012.
- (28) Vaquero, D.; Clericò, V.; Salvador-Sánchez, J.; Martín-Ramos, A.; Díaz, E.; Domínguez-Adame, F.; Meziani, Y. M.; Diez, E.; Quereda, J. Excitons, Trions and Rydberg States in Monolayer MoS₂ Revealed by Low-Temperature Photocurrent Spectroscopy. *Commun. Phys.* **2020**, *3*, No. 194.
- (29) Mak, K. F.; He, K.; Lee, C.; Lee, G. H.; Hone, J.; Heinz, T. F.; Shan, J. Tightly Bound Trions in Monolayer MoS₂. *Nat. Mater.* **2013**, *12*, 207–211.
- (30) Mawlong, L. P. L.; Bora, A.; Giri, P. K. Coupled Charge Transfer Dynamics and Photoluminescence Quenching in Monolayer MoS₂ Decorated with WS₂ Quantum Dots. *Sci. Rep.* **2019**, *9*, No. 19414.
- (31) Goswami, T.; Rani, R.; Hazra, K. S.; Ghosh, H. N. Ultrafast Carrier Dynamics of the Exciton and Trion in MoS₂ Monolayers Followed by Dissociation Dynamics in Au@MoS₂ 2D Hetero-interfaces. *J. Phys. Chem. Lett.* **2019**, *10*, 3057–3063.
- (32) Golovynskyi, S.; Irfan, I.; Bosi, M.; Seravalli, L.; Datsenko, O. I.; Golovynska, I.; Li, B.; Lin, D.; Qu, J. Exciton and Trion in Few-Layer MoS₂: Thickness- and Temperature-Dependent Photoluminescence. *Appl. Surf. Sci.* **2020**, *515*, No. 146033.
- (33) Hippalgaonkar, K.; Wang, Y.; Ye, Y.; Qiu, D. Y.; Zhu, H.; Wang, Y.; Moore, J.; Louie, S. G.; Zhang, X. High Thermoelectric Power Factor in Two-Dimensional Crystals of MoS₂. *Phys. Rev. B* **2017**, *95*, No. 115407.
- (34) *Luminescent Materials and Applications*; In Kitai, A., Ed.; Wiley Series in Materials for Electronic and Optoelectronic Applications; Wiley: Chichester, 2008.
- (35) Hernandez, Y.; Nicolosi, V.; Lotya, M.; Blighe, F. M.; Sun, Z.; De, S.; McGovern, I. T.; Holland, B.; Byrne, M.; Gun'Ko, Y. K.; Boland, J. J.; Niraj, P.; Duesberg, G.; Krishnamurthy, S.; Goodhue, R.; Hutchison, J.; Scardaci, V.; Ferrari, A. C.; Coleman, J. N. High-Yield Production of Graphene by Liquid-Phase Exfoliation of Graphite. *Nat. Nanotechnol.* **2008**, *3*, 563–568.
- (36) Gaur, A. P. S.; Sahoo, S.; Ahmadi, M.; Dash, S. P.; Guinel, M. J.-F.; Katiyar, R. S. Surface Energy Engineering for Tunable Wettability through Controlled Synthesis of MoS₂. *Nano Lett.* **2014**, *14*, 4314–4321.
- (37) Pearson, R. G. Absolute Electronegativity and Absolute Hardness of Lewis Acids and Bases. *J. Am. Chem. Soc.* **1985**, *107*, 6801–6806.
- (38) Lin, J. D.; Han, C.; Wang, F.; Wang, R.; Xiang, D.; Qin, S.; Zhang, X.-A.; Wang, L.; Zhang, H.; Wee, A. T. S.; Chen, W. Electron-Doping-Enhanced Trion Formation in Monolayer Molybdenum Disulfide Functionalized with Cesium Carbonate. *ACS Nano* **2014**, *8*, 5323–5329.
- (39) Bracker, A.; Stinaff, E.; Gammon, D.; Ware, M.; Tischler, J.; Park, D.; Gershoni, D.; Filinov, A.; Bonitz, M.; Peeters, F.; Riva, C. Binding Energies of Positive and Negative Trions: From Quantum Wells to Quantum Dots. *Phys. Rev. B* **2005**, *72*, No. 035332.
- (40) Golovynskyi, S.; Bosi, M.; Seravalli, L.; Li, B. MoS₂ Two-Dimensional Quantum Dots with Weak Lateral Quantum Confinement: Intense Exciton and Trion Photoluminescence. *Surf. Interfaces* **2021**, *23*, No. 100909.
- (41) Bora, A.; Mawlong, L. P. L.; Das, R.; Giri, P. K. Understanding the Excitation Wavelength Dependent Spectral Shift and Large Exciton Binding Energy of Tungsten Disulfide Quantum Dots and Its Interaction with Single-Walled Carbon Nanotubes. *J. Colloid Interface Sci.* **2020**, *561*, 519–532.
- (42) Kuo, Y.; Hsu, T.-Y.; Wu, Y.-C.; Hsu, J.-H.; Chang, H.-C. In *Fluorescence Lifetime Imaging Microscopy of Nanodiamonds in Vivo*, Proceedings: Advances in Photonics of Quantum Computing, Memory, and Communication VI, Hasan, Z. U.; Hasan, Z. U.; Hemmer, P. R.; Lee, H.; Santori, C. M., Eds.; San Francisco, CA, 2013; p 863503.